

# Scanning Electrochemical Microscopy. 19. Ion-Selective Potentiometric Microscopy

Benjamin R. Horrocks, Michael V. Mirkin, David T. Pierce,<sup>†</sup> and Allen J. Bard<sup>\*</sup>

Department of Chemistry and Biochemistry, The University of Texas at Austin, Austin, Texas 78712

Geza Nagy and Klara Toth

Institute for General and Analytical Chemistry, Technical University, Budapest, Hungary

**Potentiometric pH selective tips for scanning electrochemical microscopy (SECM) have been developed and used to image local pH changes in a variety of model chemical systems. Images of pH profiles around a platinum microelectrode during water reduction, a corroding disk of silver iodide in aqueous potassium cyanide, a disk of immobilized urease hydrolyzing urea, and a disk of immobilized yeast cells in glucose solution were obtained. A simple method for fabricating antimony microdisk electrodes suitable for use in SECM is described. The general theory for SECM with potentiometric ion selective tips is also presented, assuming that the tip is a purely passive sensor. Reasonable agreement with theory was observed for relatively large tip to surface separations. The deviations observed at small separations were due to shielding of the surface by the tip and, consequently, were found to be much less significant for smaller tips.**

## INTRODUCTION

Scanning electrochemical microscopy (SECM) has already proved to be a valuable tool for obtaining surface chemical information with high spatial resolution.<sup>1,2</sup> In SECM amperometry, the effect of the surface of the sample on the diffusion-controlled electrochemical reaction of a mediator at an ultramicroelectrode tip is measured. The mediator is usually, though not necessarily, a part of a reversible redox couple. Images are produced by scanning the ultramicroelectrode tip over the surface using precision piezoelectric micropositioners. These images reflect the different mechanisms by which the sample surface can affect the tip current. The current at the tip is sensitive to the tip-surface distance and chemical or electrochemical reactions at the tip and the surface.

For a reversible redox couple, the tip current decreases as the tip approaches an insulator because the surface blocks diffusion to the electrode. However, near a conductor the current increases with decreasing separation because of the recycling of the redox couple at the surface; this effect is known as positive feedback.<sup>3</sup> The dependence of the tip current on the tip to surface separation has been calculated

for both conductive and insulating surfaces. Topographic imaging of a variety of surfaces, including metals,<sup>4</sup> conducting polymers,<sup>5</sup> Nafion,<sup>6</sup> microelectrode arrays,<sup>7</sup> filter membranes, and biological samples such as leaves<sup>8</sup> and filaments of algae<sup>1</sup> has been demonstrated. Samples containing both insulating and conducting regions can also be studied, and the effects of topography and conductivity can be separated by modulating the tip position and measuring the modulated component of the tip current with a lock-in amplifier.<sup>9</sup>

A particular advantage of the SECM over other scanning probe microscopes is that the tip current is also influenced by chemical processes at the surface or in the solution. For example, the faradaic reaction at the tip can perturb an adsorption equilibrium at an insulating surface. Desorption of electroactive species from the surface produces an increase in the tip current over that expected for an inert insulator. This effect has been used to study the rate of desorption and surface diffusion of hydrogen ions at a titanium dioxide surface.<sup>10</sup> If the rate of mediator turnover at a conducting surface is not diffusion controlled, the SECM image can then reflect the local electrode kinetics at different regions of a conductor due to the presence of catalysts or passivating layers. Active sites for electron transfer on a surface produce a greater enhancement of the current at the tip, and catalytic gold particles on a glassy carbon surface have been imaged using this effect.<sup>11,12</sup> A similar effect occurs if the mediator is recycled by a surface-immobilized redox active species. The oxidoreductases are a large class of redox active enzymes. These enzymes catalyze redox reactions of a specific substrate with a coenzyme or cosubstrate. By using a high substrate concentration, the enzyme can be kept either fully reduced or fully oxidized. In the absence of the natural redox partner of the enzyme, a tip-generated mediator can be used to monitor the enzyme activity on the surface. The tip current then depends on the kinetics of the regeneration of the mediator by the enzyme. Recent work has shown that the distribution of enzymes on biological samples (rat liver mitochondria) and the kinetics of surface-immobilized glucose oxidase can be measured.<sup>1,13</sup>

Unfortunately, many interesting chemical systems are not accessible to amperometric techniques. As an example, alkali and alkaline earth metal ion profiles are particularly important

<sup>†</sup> Present address: Department of Chemistry, University of North Dakota, Grand Forks, ND 58202.

(1) Bard, A. J.; Fan, F.-R. F.; Pierce, D. T.; Unwin, P. R.; Wipf, D. O.; Zhou, F. *Science* **1991**, *254*, 68.

(2) Bard, A. J.; Denault, G.; Lee, C.; Mandler, D.; Wipf, D. O. *Acc. Chem. Res.* **1990**, *23*, 357.

(3) Kwak, J.; Bard, A. J. *Anal. Chem.* **1989**, *61*, 1221.

(4) Kwak, J.; Bard, A. J. *Anal. Chem.* **1989**, *61*, 1794.

(5) Kwak, J.; Lee, C.; Bard, A. J. *J. Electrochem. Soc.* **1990**, *137*, 1481.

(6) Jeon, I. C.; Anson, F. C. *Anal. Chem.* **1992**, *64*, 2021.

(7) Lee, C.; Miller, C. J.; Bard, A. J. *Anal. Chem.* **1991**, *63*, 78.

(8) Lee, C.; Kwak, J.; Bard, A. J. *Proc. Natl. Acad. Sci. U.S.A.* **1990**, *87*, 1740.

(9) Wipf, D. O.; Bard, A. J. *Anal. Chem.* **1992**, *64*, 1362.

(10) Unwin, P. R.; Bard, A. J. *J. Phys. Chem.* **1992**, *96*, 5035.

(11) Wipf, D. O.; Bard, A. J. *J. Electrochem. Soc.* **1991**, *138*, L4.

(12) Wipf, D. O.; Bard, A. J. *J. Electrochem. Soc.* **1991**, *138*, 469.

(13) Pierce, D. T.; Unwin, P. R.; Bard, A. J. *Anal. Chem.* **1992**, *64*, 1795.

in experimental life science but cannot be quantified by voltammetry in aqueous media. Furthermore, simple amperometric detection methods have poor chemical selectivity, and the addition of a redox couple to the medium required by the technique can perturb the system under study. In the life sciences, many different ion-selective potentiometric microelectrodes have been used to measure local ion activity in biological microstructures sometimes as small as organelles.<sup>14</sup> To broaden the scope of SECM, an obvious possibility is the use of an ion-selective potentiometric sensor as the scanning probe. Work in this area is in progress in several laboratories. The use of a silver/silver chloride microelectrode to study chloride ion fluxes at a polyaniline-coated electrode has been reported.<sup>15</sup> A study of one-dimensional pH and chloride ion profiles in corrosion pits on metals has also been reported, but at much lower resolution than that of SECM.<sup>16</sup> A scanning reference electrode has also been used to map distributions of potential over corroding metals with a spatial resolution on the order of millimeters.<sup>17,18</sup> In comparing the abilities of amperometric and potentiometric modes of SECM, it should be remembered that while amperometric SECM relies on the interaction of the system with the chemical species generated at the tip, potentiometric detection requires the existence of concentration profiles between the surface and the bulk of solution. In other words, potentiometric detection is only possible if there are local ion activity profiles in the system under investigation. If the system is at steady state, an image of these ion activity profiles can be made by scanning the potentiometric tip across the surface in the usual way.

A broad class of reactions involves pH changes, and therefore, we have concentrated on the development of pH-selective microelectrodes suitable for use in SECM as a first step. Many enzyme reactions, corrosion processes, electrochemical reactions, and metabolic processes of microorganisms involve pH changes. Recently, the combination of a pH-sensitive fluorescent dye and a fluorescence microscope has been successfully used to image the pH around metal electrodes during water reduction and during corrosion.<sup>19</sup> The use of a potentiometric pH sensor in SECM has the advantage of providing directly the local pH as well as the pH profiles normal to the sample surface.

In the life sciences, several different designs for small pH electrodes have been successfully employed.<sup>20-22</sup> In the early studies, glass membrane microelectrodes gained application, but have since been superseded by the glass micropipet-based sensors.<sup>14</sup> In studies of living systems, the location of the measuring tip is determined either by optical microscopy or by the effect of the system on the electrode, e.g., the potential change when the tip penetrates a cell. An advantage of amperometric SECM is the use of the signal itself to determine the absolute tip to surface distance. This cannot be done with tips such as the glass membrane electrodes or micropipets. The effective use of potentiometric tips in SECM requires an independent distance measurement. In some cases this can be done with an optical microscope;<sup>15</sup> however,

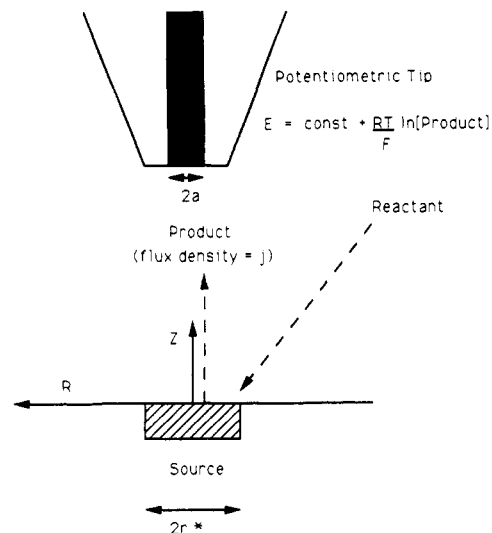


**Figure 1.** Schematic of the concentration profile around a microdisk source and the measurement of the profile with a potentiometric SECM tip. The product of the reaction at the microdisk source diffuses into solution. The concentration profile of the product that develops is monitored by measuring the potential of the ion-selective tip against a reference electrode in the bulk solution. In contrast to amperometric SECM, the concentration profile is produced by the sample and not by the tip.

this is usually not practical, especially for micrometer-sized tips. The ideal solution is to have a tip electrode that can be operated in both amperometric and potentiometric modes. After using the amperometric function of the tip to approach the surface and calibrate the distance or to do topographical imaging, potentiometric ion-selective imaging can be performed. To achieve this, different approaches can be considered, such as multibarrel sensors with separate voltammetric and potentiometric electrodes on the same tip and metal/metal oxide sensors. In our preliminary work, antimony electrodes were found to be very promising in this respect. Antimony pH sensors are broadly used in different areas as an alternative to glass electrodes, e.g., in fluoride media or in the food industry where glass electrodes are not permitted due to the danger of contaminating the food with glass fragments. The properties of antimony electrodes have been reviewed recently,<sup>20</sup> and different kinds of antimony microelectrodes have been reported.<sup>21,22</sup> Most of these designs involve very thin-walled glass capillaries to facilitate cell penetration and minimize damage. For microscopy, a more durable and polishable design is needed. It is especially important for the exposed electrode surface to have a well-defined geometry that allows calculation of the mass transport to the electrode. In this respect the microdisk is the most suitable, since the theory for amperometric measurements with this geometry is already available.<sup>3</sup>

We describe here the fabrication of antimony microdisk electrodes and their use as potentiometric tips for SECM. A simple theoretical model for the technique is proposed, and the problems associated with this technique are discussed. Some examples of the successful potentiometric pH imaging of electrochemical, corroding, enzymatic, and biological systems are also presented.

## THEORY

Unlike the amperometric feedback SECM mode, in potentiometric experiments the tip is a passive sensor, i.e., it does not affect the concentration profile of species generated (or consumed) chemically or electrochemically at the substrate (Figure 1). Thus, in principle, the theory for potentiometric

(14) Ammann, D. *Ion Selective Microelectrodes: Principles, Design and Application*; Springer: New York, 1986.

(15) Denault, G.; Troise-Frank, M. H.; Peter, L. M. *Faraday Discuss. Chem. Soc.* 1992, 94.

(16) Luo, J. L.; Lu, Y. C.; Ives, M. B. *J. Electroanal. Chem. Interfacial Electrochem.* 1992, 326, 51.

(17) Isaacs, H. *NACE Localized Corrosion* 1974, 3, 158.

(18) O'Halloran, R. J.; Williams, L. F. G.; Lloyd, C. P. *NACE Localized Corrosion* 1984, 40, 344.

(19) Engstrom, R. C.; Chaffari, S.; Qu, H. *Anal. Chem.* 1992, 64, 2525.

(20) Glab, S.; Hulanicki, A.; Edwall, G.; Ingman, F. *Crit. Rev. Anal. Chem.* 1989, 21, 29.

(21) Bicher, H. A.; Ohki, S. *Biochim. Biophys. Acta* 1972, 255, 900.

(22) Matsumura, Y.; Kajino, K.; Fujimoto, M. *Membr. Biochem.* 1980, 3, 99.

SECM should be simpler than that for the amperometric feedback mode.<sup>1</sup> Here, we consider only the steady-state model, because the potentiometric sensors are generally unsuitable for fast transient measurements. While a flat source of electroactive species (e.g., a microdisk substrate) is more convenient, it is not always possible to prepare such substrates. Therefore, two types of the source geometry will be considered: a microdisk and a hemisphere. If the products produced at the source are stable and do not participate in a homogeneous reaction in solution, the time-independent diffusion problem can be formulated by the following equations for a hemisphere:

$$\nabla^2 C(R) = 0 \quad (1)$$

$$R \rightarrow \infty; C(R) \rightarrow C^* \quad (2)$$

$$R = r^*; j(r^*) = -D(\partial C/\partial R)_{R=r^*} \quad (3)$$

For a microdisk:

$$\nabla^2 C(R,Z) = 0 \quad (4)$$

$$R + Z \rightarrow \infty; C(R,Z) \rightarrow C^* \quad (5)$$

$$Z = 0, 0 \leq R \leq r^*; j(R) = -D(\partial C/\partial Z); Z = 0; r^* < R; \partial C/\partial Z = 0 \quad (6)$$

where  $C$  and  $C^*$  are the concentration of the product species and its bulk value, respectively;  $r^*$  is the source radius;  $D$  is the diffusion coefficient; and  $j$  is the flux density.  $\nabla^2$  is the Laplacian operator in spherical (eq 1) or cylindrical (eq 4) coordinates. While one usually needs to find the flux to the surface by solving eqs 1–3 or eqs 4–6, our task is the opposite one, i.e., to find the concentration profile assuming that the flux is known.

The hemisphere problem (eqs 1–3) in polar coordinates can be easily solved to yield<sup>23</sup>

$$C = C^* + r^{*2}j/DR \quad (7)$$

Since the total flux  $J = 2\pi r^{*2}j$  one can rewrite eq 7 as

$$C = C^* + J/(2\pi DR) \quad (8)$$

For the microdisk, eq 4 in cylindrical coordinates can be solved as shown in the Appendix. The dimensionless concentration profiles above a microdisk, i.e., the function  $c(r,z)/f$ , were computed from eqs A5 and A8 (see Appendix) and compared. As expected, the differences are minor and can be detected only at quite small tip–substrate separations ( $z < 1$ ). Since the fit of the experimental data to the theory in this region is difficult because of tip shielding (see below), we neglect these differences and use only eqs A5 and A6 to interpret experimental results. The concentration profile  $c(r,z)/f$  given in Table I was computed from eq A5.

The potentiometric SECM experiment yields the potential of the tip electrode,  $E$ , as a function of the tip–substrate separation. To establish a correspondence between these data and the above theory, one needs to know the  $E$  vs  $C$  dependence, typically of the form

$$E = E' + S \log C \quad (9)$$

where  $E'$  is a constant and the slope,  $S$ , is equal to  $2.303 RT/nF$  ( $0.059/n$ , at 25 °C) for an ideal electrode. Using such a calibration, one can transform the experimental results to the  $C$  vs  $(z,r)$  dependence and fit them to the theoretical values of Table I to find  $J$  and confirm the distance scale. Similar procedures were described previously<sup>3,24</sup> for the feedback-mode SECM.

When the tip electrode is not small compared to the substrate, its potential is determined by the average value of concentration at the tip surface. In the case of the hemispherical substrate, the average distance from the source center to the surface is

$$\langle r \rangle = 2[(z^2 + a^2)^{3/2} - z^3]/3a^2 \quad (10)$$

where  $z$  is the distance between the tip and substrate centers and  $a$  is the ratio of the tip and substrate radii. The average value of the surface concentration can be obtained by substituting  $\langle r \rangle$  in eq 7. When the substrate is a microdisk, the approximate average value of the surface concentration can be computed from Table I according to the formula

$$\langle c \rangle = \frac{2}{a^2} \int_0^a c(r)r dr \quad (11)$$

While the theory outlined above is simpler than the theory of the amperometric feedback mode, fitting the experimental data is not so straightforward. Unlike the feedback mode, where the diffusion layer is confined to a narrow gap between the tip and substrate electrodes, in the present case the inert tip moves within the thick diffusion layer created by the substrate reaction. Thus, the effects of substrate screening and stirring of the diffusion layer by the tip will prevent one from obtaining a quantitative fit between theory and experiment at close tip–substrate separations. The above theory assumes that the species generated at the substrate is stable. In the experiments with the pH sensors described here, the thickness of the diffusion layer at the substrate was governed by the reaction of  $H^+$  (or  $OH^-$ ) with a buffer component, i.e., as the  $H^+$  diffuses away from the substrate it reacts with (“titrates”) the base form of the buffer to establish the pH gradient. The following approximate treatment can be used to account for this effect. Suppose the electrolyte contains the buffer system  $HB$  and  $B^-$  at a total concentration  $C^\circ$  and a bulk concentration of protons  $[H]_b \ll C^\circ$ . The protons formed at the substrate react with  $B^-$  as follows



and the dissociation constant is

$$K = [H^+][B^-]/[HB] \quad (13)$$

One can derive from eq A5 (and from eqs 7 or A6 as well)

$$C(r,z) = C^* + \Delta C \quad (14)$$

where  $[H]_b = C^* = K[HB]_b/[B^-]_b$ , the subscript  $b$  indicates the original (bulk) concentration of the species, and  $C^\circ = [HB] + [B^-]$ .  $\Delta C$  is the additional amount of protons that have arrived at a given point  $(r,z)$  with respect to the substrate because of the substrate reaction. We assume a buffer solution where the proton concentration is negligibly small compared to  $C^\circ$ , so that  $\Delta C$  will relate to the local changes in  $[B^-]$  and  $[HB]$ . This change can be computed as follows:

$$[B^-] = C^\circ K / ([H^+] + K) \quad (15)$$

$$\Delta C = [B^-]_b - [B^-] = C^\circ K \frac{[H^+] - [H]_b}{([H]_b + K)([H^+] + K)} \quad (16)$$

This can be solved to find  $[H^+]$  at any given point as a function of  $\Delta C$

$$[H^+] = \frac{C^\circ K [H]_b + \Delta C K ([H]_b + K)}{C^\circ K - \Delta C ([H]_b + K)} \quad (17)$$

(If  $OH^-$  is produced at the substrate,  $\Delta C$  in eq 17 is replaced by  $-\Delta C$ .) By computing  $\Delta C$  from eqs 7, A5, or A6, one can obtain the theoretical  $C$  vs  $(r,z)$  curves as a function of the flux and determine the last parameter by fitting these to the experimental data.

(23) Bard, A. J.; Faulkner, L. R. *Electrochemical Methods: Fundamentals and Applications*; Wiley: New York, 1980; pp 145–6.

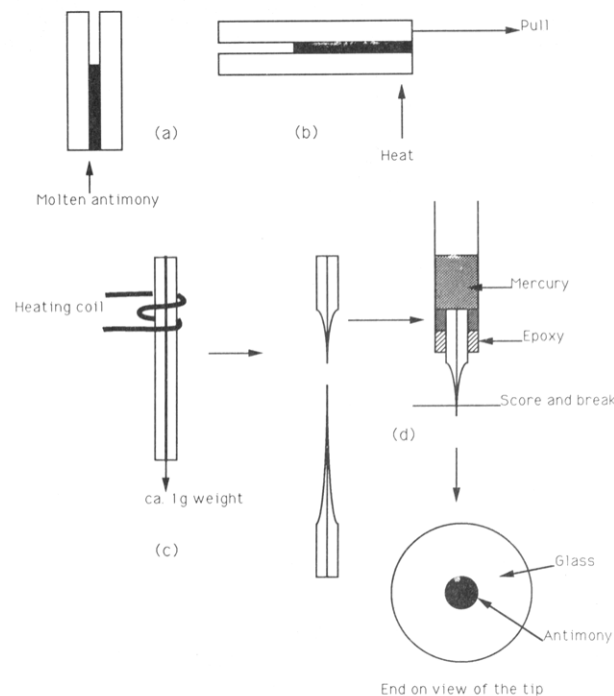
(24) Mirkin, M. V.; Fan, F.-R. F.; Bard, A. J. *J. Electroanal. Chem. Interfacial Electrochem.* 1992, 328, 47.

Table I. Dimensionless Steady-State Concentration Profile  $c(z,r)/f$  for Electroactive Species Generated at Disk-Shaped Substrate\*

$z/r$	0.0	0.1	0.2	0.3	0.4	0.5	0.6	0.7	0.8	0.9	1.0	1.1	1.2	1.3	1.4	1.5	1.6	1.7	1.8	1.9	2.0
0.05	0.9512	1.0654	1.0581	1.0384	1.0118	0.9793	0.9405	0.8941	0.8381	0.7677	0.6747	0.5648	0.4206	0.4716	0.4321	0.3993	0.3715	0.3475	0.3265	0.3080	0.2915
0.10	0.9050	1.0143	1.0093	0.9907	0.9649	0.9331	0.8951	0.8499	0.7958	0.7302	0.6523	0.5768	0.5167	0.4693	0.4305	0.3982	0.3706	0.3468	0.3259	0.3075	0.2911
0.15	0.8612	0.9644	0.9618	0.9447	0.9201	0.8894	0.8526	0.8092	0.7580	0.6980	0.6310	0.5660	0.5108	0.4655	0.4280	0.3963	0.3692	0.3457	0.3251	0.3068	0.2905
0.20	0.8198	0.9166	0.9161	0.9007	0.8775	0.8481	0.8130	0.7718	0.7240	0.6695	0.6108	0.5537	0.5033	0.4606	0.4245	0.3938	0.3673	0.3442	0.3239	0.3058	0.2897
0.25	0.7808	0.8712	0.8723	0.8587	0.8370	0.8093	0.7761	0.7373	0.6930	0.6437	0.5916	0.5407	0.4947	0.4548	0.4204	0.3907	0.3649	0.3423	0.3223	0.3046	0.2887
0.30	0.7440	0.8283	0.8308	0.8188	0.7988	0.7729	0.7416	0.7054	0.6646	0.6198	0.5732	0.5275	0.4855	0.4482	0.4155	0.3870	0.3620	0.3400	0.3205	0.3031	0.2874
0.35	0.7095	0.7880	0.7915	0.7811	0.7627	0.7386	0.7095	0.6759	0.6383	0.5976	0.5556	0.5143	0.4758	0.4410	0.4101	0.3829	0.3588	0.3374	0.3184	0.3013	0.2859
0.40	0.6770	0.7501	0.7544	0.7454	0.7287	0.7064	0.6794	0.6483	0.6138	0.5768	0.5387	0.5012	0.4659	0.4335	0.4044	0.3784	0.3552	0.3345	0.3160	0.2993	0.2843
0.45	0.6466	0.7147	0.7196	0.7118	0.6967	0.6762	0.6513	0.6226	0.5910	0.5572	0.5226	0.4884	0.4558	0.4257	0.3983	0.3735	0.3513	0.3314	0.3134	0.2972	0.2825
0.50	0.6180	0.6815	0.6868	0.6803	0.6666	0.6478	0.6249	0.5986	0.5695	0.5387	0.5071	0.4758	0.4457	0.4177	0.3919	0.3684	0.3472	0.3280	0.3106	0.2948	0.2805
0.55	0.5913	0.6504	0.6561	0.6506	0.6383	0.6212	0.6001	0.5760	0.5494	0.5212	0.4922	0.4635	0.4357	0.4096	0.3854	0.3631	0.3428	0.3244	0.3076	0.2923	0.2783
0.60	0.5662	0.6214	0.6273	0.6227	0.6117	0.5961	0.5769	0.5547	0.5303	0.5045	0.4780	0.4515	0.4259	0.4015	0.3787	0.3571	0.3383	0.3206	0.3044	0.2896	0.2760
0.65	0.5427	0.5982	0.6042	0.5995	0.5887	0.5726	0.5550	0.5347	0.5123	0.4886	0.4643	0.4399	0.4161	0.3934	0.3720	0.3521	0.3337	0.3167	0.3011	0.2868	0.2736
0.70	0.5207	0.5688	0.5749	0.5719	0.5633	0.5504	0.5344	0.5158	0.4953	0.4735	0.4511	0.4286	0.4066	0.3854	0.3653	0.3464	0.3289	0.3127	0.2977	0.2838	0.2711
0.75	0.5000	0.5450	0.5512	0.5489	0.5412	0.5296	0.5149	0.4979	0.4791	0.4592	0.4385	0.4177	0.3972	0.3774	0.3585	0.3407	0.3241	0.3085	0.2942	0.2808	0.2685
0.80	0.4806	0.5228	0.5290	0.5272	0.5204	0.5099	0.4966	0.4810	0.4638	0.4454	0.4264	0.4071	0.3881	0.3696	0.3518	0.3350	0.3192	0.3043	0.2905	0.2777	0.2658
0.85	0.4624	0.5020	0.5082	0.5069	0.5009	0.4914	0.4793	0.4650	0.4492	0.4323	0.4147	0.3969	0.3791	0.3618	0.3452	0.3293	0.3142	0.3001	0.2869	0.2745	0.2630
0.90	0.4454	0.4825	0.4886	0.4877	0.4825	0.4740	0.4629	0.4499	0.4354	0.4198	0.4035	0.3870	0.3705	0.3543	0.3386	0.3236	0.3093	0.2958	0.2831	0.2713	0.2601
0.95	0.4293	0.4642	0.4702	0.4693	0.4641	0.4575	0.4474	0.4355	0.4222	0.4078	0.3927	0.3774	0.3620	0.3468	0.3321	0.3179	0.3044	0.2915	0.2794	0.2680	0.2572
1.00	0.4142	0.4471	0.4530	0.4528	0.4488	0.4419	0.4328	0.4219	0.4096	0.3963	0.3824	0.3681	0.3538	0.3396	0.3257	0.3123	0.2994	0.2872	0.2756	0.2646	0.2543
1.10	0.3866	0.4158	0.4215	0.4219	0.4188	0.4133	0.4057	0.3966	0.3862	0.3748	0.3629	0.3505	0.3380	0.3255	0.3133	0.3013	0.2897	0.2786	0.2680	0.2579	0.2483
1.20	0.3620	0.3881	0.3935	0.3943	0.3921	0.3876	0.3813	0.3736	0.3648	0.3551	0.3448	0.3341	0.3232	0.3122	0.3013	0.2906	0.2802	0.2701	0.2604	0.2512	0.2423
1.30	0.3401	0.3635	0.3686	0.3697	0.3681	0.3645	0.3593	0.3528	0.3453	0.3370	0.3281	0.3188	0.3092	0.2995	0.2899	0.2803	0.2709	0.2618	0.2529	0.2444	0.2363
1.40	0.3205	0.3415	0.3464	0.3476	0.3465	0.3437	0.3394	0.3339	0.3275	0.3204	0.3127	0.3045	0.2961	0.2876	0.2789	0.2704	0.2619	0.2536	0.2456	0.2378	0.2302
1.50	0.3028	0.3218	0.3264	0.3278	0.3271	0.3248	0.3212	0.3166	0.3112	0.3050	0.2983	0.2912	0.2838	0.2762	0.2685	0.2609	0.2532	0.2457	0.2384	0.2312	0.2243
1.60	0.2868	0.3041	0.3084	0.3098	0.3095	0.3077	0.3047	0.3008	0.2962	0.2908	0.2850	0.2788	0.2722	0.2655	0.2587	0.2518	0.2449	0.2381	0.2314	0.2248	0.2184
1.70	0.2723	0.2880	0.2921	0.2936	0.2935	0.2921	0.2896	0.2863	0.2823	0.2777	0.2726	0.2672	0.2614	0.2554	0.2493	0.2431	0.2369	0.2307	0.2246	0.2186	0.2127
1.80	0.2591	0.2735	0.2773	0.2789	0.2789	0.2778	0.2758	0.2730	0.2696	0.2656	0.2611	0.2563	0.2512	0.2459	0.2404	0.2348	0.2292	0.2236	0.2180	0.2125	0.2071
1.90	0.2471	0.2603	0.2639	0.2654	0.2656	0.2648	0.2631	0.2608	0.2578	0.2543	0.2504	0.2462	0.2416	0.2369	0.2320	0.2269	0.2219	0.2167	0.2116	0.2066	0.2016
2.00	0.2361	0.2482	0.2516	0.2531	0.2534	0.2528	0.2515	0.2495	0.2469	0.2439	0.2404	0.2367	0.2326	0.2284	0.2240	0.2194	0.2148	0.2102	0.2055	0.2009	0.1963
2.10	0.2259	0.2371	0.2403	0.2418	0.2422	0.2418	0.2407	0.2390	0.2368	0.2341	0.2311	0.2278	0.2242	0.2204	0.2164	0.2123	0.2081	0.2039	0.1996	0.1954	0.1911
2.20	0.2166	0.2270	0.2300	0.2315	0.2319	0.2316	0.2307	0.2293	0.2274	0.2250	0.2224	0.2194	0.2162	0.2128	0.2092	0.2055	0.2017	0.1979	0.1940	0.1900	0.1861
2.30	0.2080	0.2176	0.2204	0.2219	0.2224	0.2222	0.2215	0.2203	0.2186	0.2166	0.2142	0.2116	0.2087	0.2056	0.2024	0.1991	0.1956	0.1921	0.1885	0.1849	0.1813
2.40	0.2000	0.2089	0.2116	0.2130	0.2136	0.2135	0.2129	0.2119	0.2104	0.2086	0.2066	0.2042	0.2016	0.1989	0.1960	0.1929	0.1898	0.1866	0.1833	0.1800	0.1766
2.50	0.1926	0.2009	0.2035	0.2048	0.2054	0.2054	0.2049	0.2040	0.2028	0.2012	0.1994	0.1973	0.1950	0.1925	0.1899	0.1871	0.1842	0.1813	0.1783	0.1752	0.1721
2.60	0.1857	0.1934	0.1959	0.1972	0.1978	0.1978	0.1975	0.1967	0.1956	0.1943	0.1926	0.1908	0.1887	0.1864	0.1840	0.1815	0.1789	0.1762	0.1734	0.1706	0.1678
2.70	0.1792	0.1865	0.1888	0.1901	0.1907	0.1908	0.1905	0.1899	0.1889	0.1877	0.1863	0.1846	0.1827	0.1807	0.1785	0.1762	0.1738	0.1714	0.1688	0.1662	0.1636
2.80	0.1732	0.1800	0.1822	0.1834	0.1840	0.1842	0.1840	0.1835	0.1827	0.1816	0.1803	0.1788	0.1771	0.1753	0.1733	0.1712	0.1690	0.1667	0.1644	0.1620	0.1596
2.90	0.1676	0.1740	0.1760	0.1772	0.1778	0.1780	0.1779	0.1775	0.1767	0.1758	0.1746	0.1733	0.1718	0.1701	0.1683	0.1664	0.1644	0.1623	0.1601	0.1579	0.1557
3.00	0.1623	0.1683	0.1703	0.1714	0.1720	0.1723	0.1722	0.1718	0.1712	0.1703	0.1693	0.1681	0.1667	0.1652	0.1636	0.1618	0.1600	0.1581	0.1561	0.1540	0.1519
3.20	0.1526	0.1580	0.1598	0.1608	0.1614	0.1617	0.1617	0.1614	0.1610	0.1603	0.1595	0.1585	0.1574	0.1561	0.1548	0.1533	0.1517	0.1501	0.1484	0.1467	0.1448
3.40	0.1440	0.1488	0.1504	0.1514	0.1520	0.1523	0.1523	0.1522	0.1518	0.1513	0.1507	0.1499	0.1489	0.1479	0.1468	0.1455	0.1442	0.1428	0.1414	0.1398	0.1383

3.60	0.1363	0.1406	0.1421	0.1430	0.1436	0.1439	0.1437	0.1433	0.1427	0.1421	0.1413	0.1404	0.1395	0.1384	0.1373	0.1361	0.1348	0.1335	0.1322
3.80	0.1294	0.1333	0.1346	0.1355	0.1360	0.1363	0.1364	0.1359	0.1355	0.1350	0.1343	0.1336	0.1328	0.1319	0.1309	0.1299	0.1288	0.1277	0.1265
4.00	0.1231	0.1267	0.1279	0.1287	0.1292	0.1295	0.1297	0.1293	0.1290	0.1285	0.1280	0.1274	0.1267	0.1259	0.1251	0.1242	0.1233	0.1223	0.1213
4.20	0.1174	0.1207	0.1218	0.1225	0.1230	0.1233	0.1235	0.1235	0.1233	0.1230	0.1226	0.1222	0.1217	0.1211	0.1204	0.1197	0.1189	0.1181	0.1164
4.40	0.1122	0.1152	0.1162	0.1169	0.1174	0.1177	0.1179	0.1179	0.1177	0.1175	0.1172	0.1169	0.1164	0.1159	0.1147	0.1141	0.1134	0.1126	0.1118
4.60	0.1074	0.1102	0.1112	0.1118	0.1122	0.1125	0.1127	0.1128	0.1127	0.1125	0.1123	0.1119	0.1111	0.1106	0.1101	0.1095	0.1089	0.1083	0.1076
4.80	0.1031	0.1056	0.1065	0.1071	0.1075	0.1078	0.1080	0.1081	0.1080	0.1079	0.1077	0.1074	0.1071	0.1067	0.1063	0.1058	0.1048	0.1042	0.1036
5.00	0.0990	0.1014	0.1022	0.1028	0.1032	0.1035	0.1036	0.1037	0.1037	0.1036	0.1034	0.1032	0.1029	0.1026	0.1022	0.1018	0.1009	0.1004	0.0999
5.50	0.0902	0.0921	0.0928	0.0933	0.0937	0.0939	0.0941	0.0942	0.0943	0.0943	0.0942	0.0941	0.0940	0.0938	0.0930	0.0927	0.0923	0.0920	0.0915
6.00	0.0828	0.0844	0.0850	0.0854	0.0858	0.0860	0.0862	0.0863	0.0863	0.0863	0.0862	0.0861	0.0859	0.0857	0.0855	0.0853	0.0850	0.0847	0.0844
6.50	0.0765	0.0779	0.0784	0.0788	0.0791	0.0793	0.0794	0.0795	0.0796	0.0796	0.0796	0.0795	0.0794	0.0792	0.0791	0.0789	0.0787	0.0785	0.0783
7.00	0.0711	0.0723	0.0728	0.0731	0.0733	0.0735	0.0737	0.0738	0.0739	0.0739	0.0739	0.0738	0.0737	0.0736	0.0735	0.0734	0.0732	0.0731	0.0729
7.50	0.0664	0.0674	0.0679	0.0681	0.0684	0.0685	0.0687	0.0688	0.0689	0.0689	0.0689	0.0688	0.0687	0.0686	0.0685	0.0685	0.0683	0.0682	0.0682
8.00	0.0623	0.0632	0.0636	0.0638	0.0640	0.0642	0.0643	0.0644	0.0645	0.0645	0.0645	0.0645	0.0645	0.0644	0.0644	0.0643	0.0642	0.0641	0.0640
8.50	0.0586	0.0595	0.0598	0.0600	0.0602	0.0603	0.0605	0.0606	0.0607	0.0607	0.0607	0.0607	0.0607	0.0607	0.0606	0.0606	0.0605	0.0604	0.0603
9.00	0.0554	0.0561	0.0564	0.0566	0.0568	0.0569	0.0570	0.0571	0.0572	0.0573	0.0573	0.0573	0.0573	0.0573	0.0572	0.0572	0.0571	0.0571	0.0570
9.50	0.0525	0.0532	0.0534	0.0536	0.0538	0.0539	0.0540	0.0541	0.0542	0.0542	0.0542	0.0542	0.0542	0.0542	0.0542	0.0542	0.0541	0.0541	0.0540
10.0	0.0499	0.0505	0.0507	0.0509	0.0510	0.0511	0.0512	0.0513	0.0514	0.0515	0.0515	0.0515	0.0515	0.0515	0.0515	0.0515	0.0514	0.0514	0.0513

<sup>a</sup> The flux is assumed to be uniform over the disk surface.



**Figure 2.** Schematic depicting the four stages (a-d) in the fabrication of antimony SECM tips.

## EXPERIMENTAL SECTION

**Electrode Fabrication.** The method of electrode fabrication is shown in Figure 2. Antimony shot (3–5 g, 99.999%, Aldrich, Milwaukee, WI) was melted in a small Pyrex test tube with a Bunsen flame. By use of a 50-mL syringe, molten antimony was drawn into a thick-walled Pyrex capillary (outer diameter, 7 mm; inner diameter, 1 mm) and carefully preheated in the flame (Figure 2a). The total length of the capillary was typically 25 cm, and due to solidification, the maximum continuous length of antimony inside the capillary was approximately 15 cm. With standard glassblowing techniques, antimony-filled capillaries of outside diameter in the 1–2-mm range were pulled manually. To avoid building up excess pressure in the column of antimony, the capillary was melted at the end and pulled using tweezers (Figure 2b). During this process, care must also be taken not to expose the antimony directly to the flame. After this stage, the diameter of the antimony inside the glass is in the 20–100- $\mu\text{m}$  range. In the second stage, 5-cm lengths of antimony-filled capillaries were cut and checked under the microscope to ascertain that the antimony fiber was continuous. These capillaries were pulled again using the heating coil of a microelectrode puller (Stoelting). A small weight such as a piece of glass tubing (ca. 1 g) was attached to one end of the antimony capillary. The voltage applied to the coil was set at the maximum until the capillary started to extend, then the heat was carefully reduced to obtain a thin antimony-filled capillary (Figure 2c). The short tapered upper section could then be mounted in another glass capillary as shown in Figure 2d. A well-defined disk of antimony was exposed by gently scoring near the end of the capillary and carefully breaking the capillary against a fingertip. Electrical contact was made by mercury introduced through the back of the supporting capillary. The ratio of the total tip diameter to the diameter of the antimony microdisk was typically from 5 to 10. The relatively thick glass wall of these small capillaries allows careful polishing (with MOYCO, Ultralap alumina-coated strips), and the concentric geometry of the tip allows use of previous SECM theory.<sup>3,24</sup> Antimony fibers down to about 3- $\mu\text{m}$  diameter were made into electrodes in this way, but smaller fibers were not sufficiently robust. For very thin antimony fibers, a more robust construction can be achieved by heat sealing the glass-coated antimony fibers under vacuum in low melting point glass as commonly done in

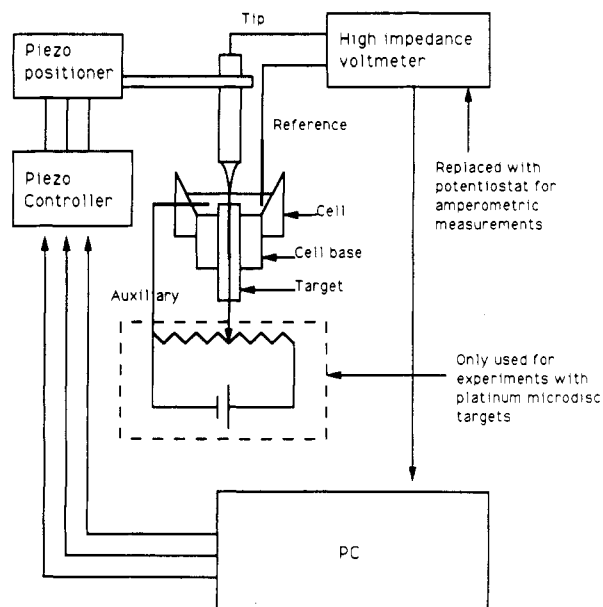


**Figure 3.** Block diagram of the SECM. The dashed box encloses a battery and potential divider used to bias the target when simultaneously measuring the SECM tip potential.

the preparation of microdisk electrodes from platinum wire.<sup>25</sup> It is important to use a low melting point capillary for this process so that the thin, Pyrex glass-coated antimony fiber does not melt during the sealing process. The tip could then be polished and beveled as described previously for voltammetric SECM tips.<sup>26</sup>

**Instrumentation.** The basic SECM instrument used in this work has been described in detail previously.<sup>4,12</sup> To allow potentiometric measurements, some small modifications were made. A block diagram of the revised microscope is shown in Figure 3. A micropositioning device (Burleigh Instruments, Fishers, NY), connected to the PC via a DAC, controls the movement of three piezoelectric inchworm motors. The cell is mounted on the horizontal ( $x$ - $y$ ) stage, and the tip is mounted on the vertical ( $z$ ) piezo. For amperometric measurements, the potential of the tip was controlled by an EI-400 bipotentiostat (Ensmann Instruments, Bloomington, IN). The output of the potentiostat was interfaced to the computer via an ADC board. A home-built high-impedance voltmeter was used to measure the potential of the tip with respect to a conventional silver/silver chloride reference. The output of the high-impedance voltmeter was fed directly into one of the ADC channels to allow acquisition of the data by the computer. When potential control of the sample and simultaneous measurement of the potential of the tip was required, a simple battery and potential divider was connected between the sample and the auxiliary electrode. The bipotentiostat was not used in this case to avoid problems arising from the interaction of the ground of the potential measuring device and the bipotentiostat. The cell was constructed from Teflon and had a volume of approximately 4 mL.<sup>13</sup> The sample (see below) was mounted in the cell base (Teflon) which screwed into the cell body. The auxiliary electrode was a piece of platinum wire, and for amperometric measurements, a separate silver/silver chloride reference electrode was used. Unless otherwise stated, all potentials are reported against silver/silver chloride in 0.1 M KCl, and the tip scan rate was 10  $\mu\text{m/s}$ . Electrochemical characterization of antimony electrodes was performed with a BAS 100A potentiostat, and pH was measured with an Orion pH meter (Model 701A).

**Targets.** Model surfaces to demonstrate potentiometric imaging were constructed as inlaid microdisk targets, because the concentration profile around such a microdisk target reaches a true steady state, as discussed in the theory section. To prepare these targets, glass capillaries were sealed at one end in a flame

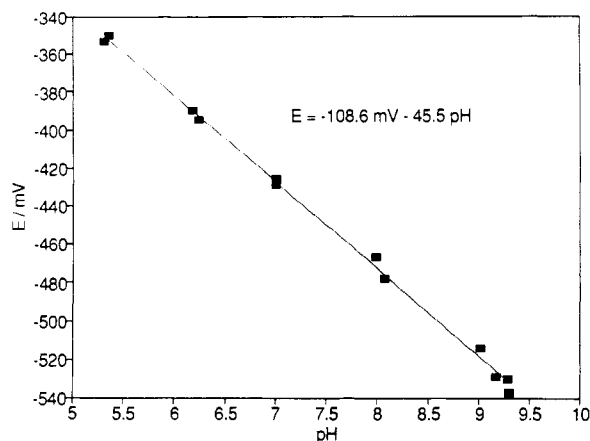


**Figure 4.** Typical calibration plot of potential against pH for a 6- $\mu\text{m}$  diameter antimony SECM tip in phosphate buffers.

with slow rotation to achieve a gradual tapering of the capillary bore toward the sealed end. The sealed end was then polished back to expose a small circular opening (diameter 25–120  $\mu\text{m}$ ) in the middle of a flat glass surface of roughly 2-mm diameter. These capillaries could then be back-filled with the chemical system of interest and finely repolished if necessary. The details of filling the targets with immobilized enzymes, yeast cells, and silver iodide are given in the discussion of the individual chemical systems. After filling, the capillary was inserted into the cell through a hole drilled in the center of the cell base. Some experiments required microdisk electrodes as targets, and these were prepared by heat sealing platinum wires (Goodfellow Metals, Cambridge, U.K.) in Pyrex capillaries (2-mm o.d.) under vacuum by conventional techniques.<sup>25</sup> After polishing, the microelectrode targets were inserted into the base of the cell as outlined above.

**Chemicals.** Urease (EC 3.5.1.5; type IX from Jack Beans, 62 IU  $\text{mg}^{-1}$ ) and bovine serum albumin (BSA; 98–99%) were obtained from Sigma Chemical Co. (St. Louis, MO). Ordinary moist baker's yeast was purchased from a grocery store. Ultra low temperature gelling agarose (United States Biochemical Corp., Cleveland, OH) was used for yeast immobilization. Biological-grade glutaraldehyde for enzyme immobilization was obtained from Polysciences, Inc. (Warrington, PA) as a 25% solution in water. Antimony shot (99.999%) was purchased from Aldrich (Milwaukee, WI). All other chemicals were of reagent grade or better, and phosphate buffers were prepared in the usual way.

## RESULTS AND DISCUSSION

**Electrode Characterization.** The pH response of a typical antimony microdisk electrode in phosphate buffer is shown in Figure 4. Some previous reports have suggested that the potential of an antimony electrode is affected by the phosphate concentration. However, no significant effect was observed for these microelectrodes for pH 7.0 phosphate buffer concentrations in the range of 1–100 mM, in agreement with the results of Glab et al.<sup>20</sup> The slopes of the calibration curves were typically between 40 and 50 mV per pH unit, which is the usual response found for polycrystalline antimony. No increase in the pH sensitivity could be achieved by oxidizing the antimony by soaking in permanganate or dichromate solutions or by anodization. The electrodes were therefore used for imaging experiments with no further pretreatment. However, after use as a voltammetric electrode for tip-surface distance measurement at negative potentials, the pH function deteriorated (the potential drifted, and the slope was significantly decreased). This problem was easily avoided by returning the electrode potential to 0 V for a few seconds before switching to potentiometric operation. The original pH function was then found to be completely restored. Reproducible behavior was observed for any individual electrode; the calibration plots were found to be within a few

(25) Wightman, R. M.; Wipf, D. O. In *Electroanalytical Chemistry*; Bard, A. J., Ed.; Marcel Dekker: New York, 1988; Vol. 15.

(26) Bard, A. J.; Fan, F.-R. F.; Kwak, J.; Lev, O. *Anal. Chem.* 1989, 61, 132.

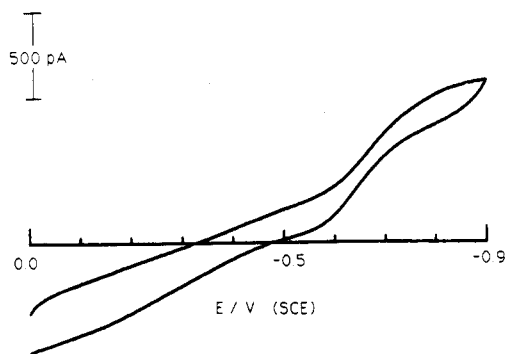


**Figure 5.** Cyclic voltammogram of a 3- $\mu\text{m}$  diameter antimony SECM tip in air-saturated 0.1 M KCl and 1 mM pH 7.0 phosphate buffer. The reference electrode was a saturated calomel electrode, and the sweep rate was 100 mV/s.

millivolts when measured on different days. It is well-known that antimony electrodes are sensitive to the presence of redox couples, and this must be taken into consideration when employing these electrodes as pH sensors.

Figure 5 shows a cyclic voltammogram of an antimony microelectrode in air-saturated pH 7.0 phosphate buffer. The oxygen reduction wave is clearly defined in the CV, and on setting the electrode potential more negative than  $-0.7$  V, a steady-state oxygen reduction current is obtained, as expected for a microelectrode. This current clearly reflected oxygen concentration changes induced by nitrogen purging or subsequent oxygen bubbling. The magnitude of the current was roughly in agreement with that expected on the basis of the usual equation for a diffusion-controlled reaction at a microdisk (assuming a 4  $e^-$  reaction). Two tip current-distance ( $i_T - d$ ) curves over a Teflon surface are shown in Figure 6. As shown, the current has a constant value, if the electrode is far from the surface. However, on approaching the surface it decreases because the reaction is totally irreversible. This negative feedback, as is also found with reversible redox couples over insulators, is the result of the shielding effect of the electrode insulation and the surface blocking the oxygen diffusion to the antimony disk. The amperometric behavior, which is in good agreement with the theory,<sup>3,24</sup> allows the measurement of absolute tip-surface distance. This distance calibration is very convenient, and no knowledge of the diffusion coefficient, concentration, or stoichiometry for the electrochemical reduction of oxygen is required. We chose to use the reduction of oxygen to determine the tip-surface distance, because this avoids the need to add an additional redox couple to the solution, which could alter the rest potential of the antimony and interfere with the pH measurement.

A typical experiment was carried out in the following manner. First, the tip was roughly positioned over the target using the  $x$ - $y$  piezos and was observed through a telescopic lens if necessary. Then air-saturated buffer solution was introduced into the cell. The tip was then operated in the amperometric mode at  $-0.8$  V and brought close to the surface using the blocking effect of the surface on the oxygen reduction current. By fitting the  $i_T - d$  data to the theoretical working curve, we can determine the absolute tip-surface distance from the measured current decrease. This is essential for quantitative measurements using the SECM. The tip was then returned to 0 V for a few seconds to reoxidize the surface of the antimony before switching to the potentiometric mode. This was necessary to restore the original pH function of the tip as described above. After the tip had been brought to a known distance from the surface, the tip was switched to the potentiometric mode. Next, the surface was systematically searched using the  $x$  and  $y$  piezo drives, and the

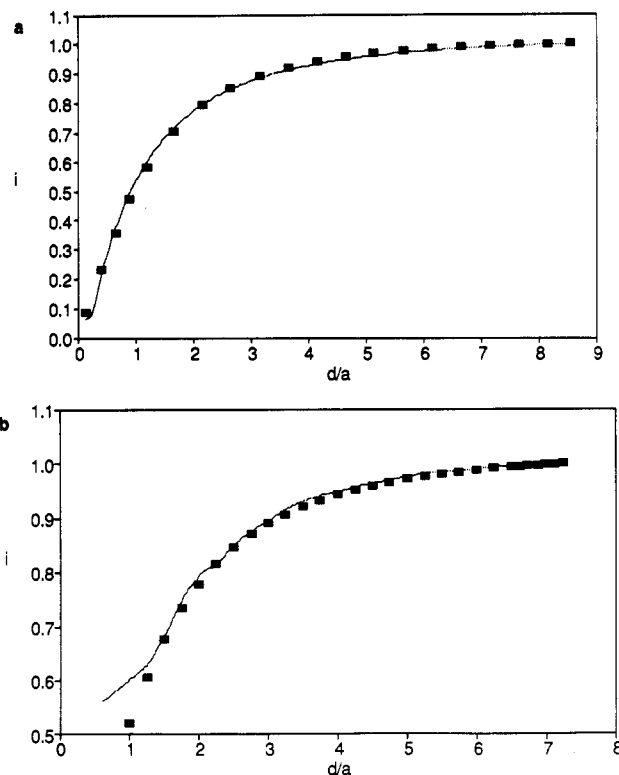
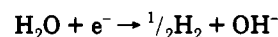


**Figure 6.** Current-distance ( $i_T - d$ ) ( $i_T$  normalized to  $i_{T,\infty}$  and  $d$  to the radius of the tip,  $a$ ) for antimony SECM tips operating in the amperometric mode. The sample surface was a Teflon disk. The solution contained 0.1 M KCl and 0.1 M pH 7.0 phosphate buffer, and the electrode potential was  $-0.8$  V. The solid line is experimental data, and the filled squares are theoretical data: (a) 40- and (b) 4- $\mu\text{m}$ -diameter antimony microdisk.

potential of the tip was monitored to observe the pH profile around the target. The approximate center of the target was located by adjusting the position of the tip in the  $X,Y$  plane to obtain the maximum difference between the local and the bulk pH. Then the tip was moved in the  $Z$  direction to determine the dependence of pH on the distance from the surface. Finally, images of the pH profile in the  $X,Y$  plane at a constant height were collected by rastering the tip across the surface in the usual manner. The response time of the tip to a pH change was not determined, but past work has indicated that metallic ion-selective electrodes typically show response times in the millisecond range.<sup>27</sup>

**Electrochemically Generated pH Profiles.** Electrochemical reactions often cause local pH changes at the electrode surface, especially if the buffer capacity of the solution is low. As a model system we chose the reduction of water at an inert microdisk electrode (25- $\mu\text{m}$  diameter platinum). As media, pH 7.0 phosphate buffers containing 0.1 M KCl were employed. To generate a pH profile, the microdisk substrate was held at a potential corresponding to the reduction of water. Care was taken not to evolve hydrogen at a rate that bubbles formed on the electrode surface; these would stir the solution near the electrode and perturb the pH measurements. In this system the electrode reaction



occurs, and the  $\text{OH}^-$  generated diffuses from the electrode surface and reacts with the acidic component of the buffer (i.e.,  $\text{H}_2\text{PO}_4^-$ ). At large tip-surface separations, the potential of the tip was offset by less than 1 mV on switching the current on, and therefore, no correction of the measured pH was made

(27) Linder, E.; Toth, K.; Pungor, E. *Dynamics of Ion Selective Electrodes*; CRC Press: Boca Raton, FL, 1988.

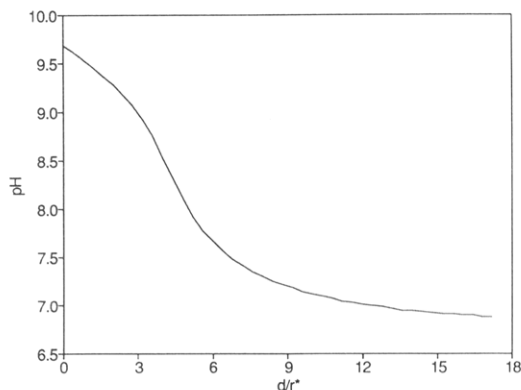


**Figure 7.** pH profile over a 25- $\mu\text{m}$ -diameter platinum disk reducing water. The solution contained 1 mM pH 7.0 phosphate buffer and 0.1 M KCl. The potential of the platinum substrate was about  $-2\text{ V}$  against a platinum auxiliary electrode, and the current was  $0.5\ \mu\text{A}$ . The profile was measured with a 40- $\mu\text{m}$ -diameter tip. The  $x$ -axis is the tip-surface distance normalized by the radius of the platinum target.

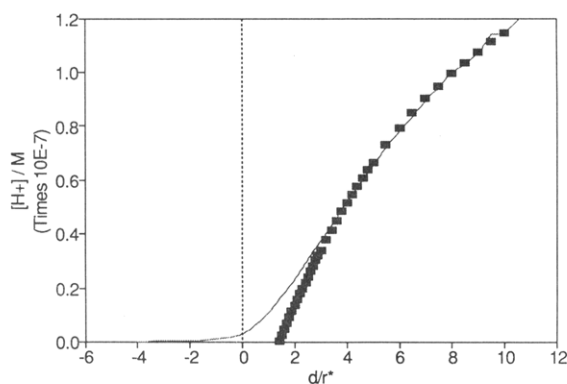


**Figure 8.** Theoretical analysis of the data of Figure 7. The  $x$ -axis is the tip-surface distance normalized by the radius of the platinum target, and the  $y$ -axis is the hydrogen ion concentration derived from the antimony potential. The solid line is experimental data, and the filled squares are theoretical data.

in these experiments. However, in less conductive solutions or in the presence of higher currents, a correction for the potential drop between the tip and the reference due to the current flowing through the solution may be necessary.<sup>15</sup>

Figure 7 shows the pH-distance profile above a platinum microdisk measured with a 40- $\mu\text{m}$ -diameter Sb tip in a 1 mM phosphate buffer at pH 7.0. The hydrogen ion concentration profile derived from this measurement is shown in Figure 8. As expected, a reasonable fit between the theory and the experiment was obtained for  $d/r^*$  values above 3, although at close separations, the influence of such a large tip prevents one from obtaining quantitative agreement. One should note the possibility of determining the distance scale from such an experiment. This may be important for other ion-selective sensors which cannot be used voltammetrically in the same way as antimony.

Figure 9a,b shows images of the pH profile around a 25- $\mu\text{m}$  platinum disk at two higher concentrations of pH 7.0 phosphate buffer. An enlarged, slightly oval image of the target disk can be clearly recognized in both pictures. As can be easily seen, in the lower buffer capacity solution, the magnitude of the pH change is greater, but the image is more diffuse and enlarged. This effect of the buffer capacity on the image can easily be understood. The shift in pH near the electrode surface is due to the titration of the buffer with the hydroxide anions produced at the electrode surface. Therefore, as the buffer capacity is increased, a higher concentration of hydroxide must be generated to achieve the same pH change. At lower buffer capacity, the pH change can spread

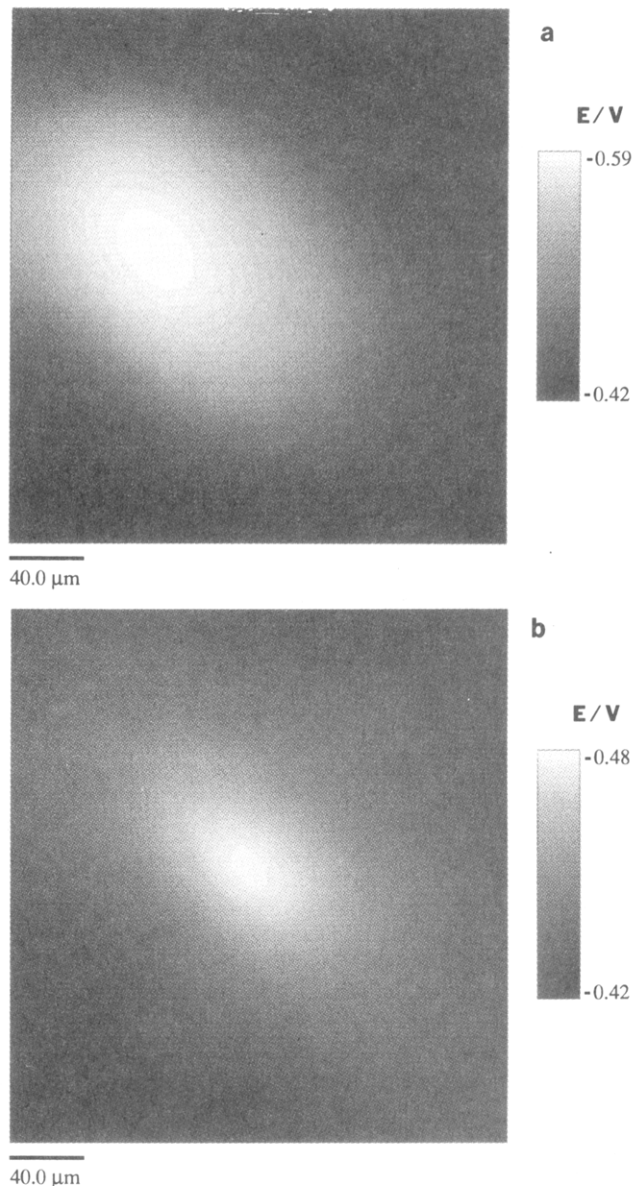


**Figure 9.** Images of the pH profile around a 25- $\mu\text{m}$  platinum target reducing water. The gray scale shows the antimony tip potential; white corresponds to high pH. The potential of the target was  $-2\text{ V}$  versus a platinum auxiliary, and the current was  $0.5\ \mu\text{A}$ . In both cases, the diameter of the antimony tip was 40  $\mu\text{m}$ , the tip-surface distance was 33  $\mu\text{m}$ , and the tip scan rate was 10  $\mu\text{m}/\text{s}$ . The solutions contained 0.1 M KCl and pH 7.0 phosphate buffer in two different concentrations: (a) 5 and (b) 20 mM buffer.

over a greater volume of solution before being quenched. The dependence of the observed "image broadening" upon the buffer capacity can be calculated theoretically. Figure 10 displays three  $[\text{H}^+]$  vs  $r$  curves calculated for different values of the buffer capacity but the same bulk pH value (the substrate is the microdisk generating a constant flux of  $\text{OH}^-$  ions independent of the buffer concentration). At higher buffer concentration (30 mM, the upper curve),  $[\text{H}^+]$  reaches about 90% of its bulk value at  $r = 2$ . Thus, the apparent image should be about twice as large as the original substrate. At lower buffer concentrations (10 mM, the middle curve, and 3 mM, the lower curve), the values of  $[\text{H}^+]$  at  $r = 2$  are only about 70% and 40% of the bulk value; therefore, the corresponding images would appear much larger. Although with the known flux and other experimental parameters one can try to account for diffusional broadening and evaluate the true substrate size, potentiometric imaging in strongly buffered solutions (or with a short-lived mediator) seems to



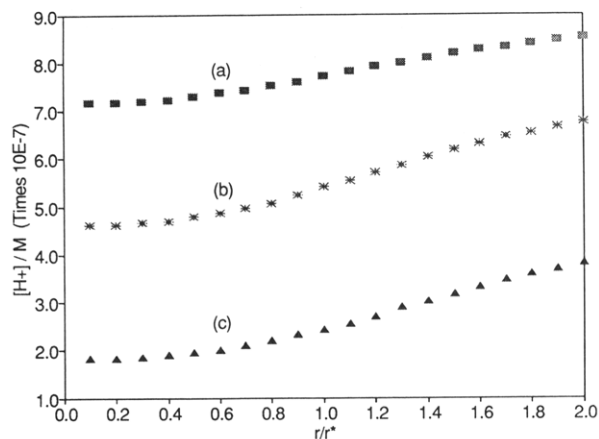
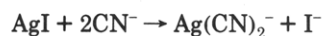


**Figure 10.** Theoretical hydrogen ion concentration profiles across a microdisk generating a constant flux of hydroxide in pH 6 1:1 buffer of total concentration: (a) 30, (b) 10, and (c) 3 mM.

be advantageous. On the contrary, kinetic studies should be carried out with a stable potential-determining species to allow the use of the above exact theory.

**Corrosion of Silver Iodide.** The corrosion of silver halides in aqueous potassium cyanide is thought to be responsible for the operation of silver halide-based solid-state cyanide-selective electrodes.<sup>28</sup> The mechanism of these sensors has excited considerable interest.<sup>28-30</sup> It has been suggested that a local pH change due to the consumption of cyanide anion at a silver iodide surface by complexation with silver



is responsible for some unusual features of the behavior observed in low buffer capacity solutions.<sup>29</sup> An obvious possible use of potentiometric SECM was to address this question directly.

In our work, silver iodide powder was introduced into the glass capillaries described in the Experimental Section. The powder was carefully melted in a Bunsen flame and was forced to the end of the capillary by vigorous shaking. After the tube had cooled, the surface was repolished with successively finer grades of alumina (1  $\mu\text{m}$ , 0.3  $\mu\text{m}$ , and finally 0.05  $\mu\text{m}$ ) to expose a silver iodide disk of diameter in the range of 40–80  $\mu\text{m}$ . The experimental procedure was the same as for the experiments described above except that the silver iodide target was at open circuit. Measurements were made in 1 mM potassium cyanide solutions containing 100 mM potassium chloride and pH 9 phosphate buffer in different concentrations. Figure 11 shows a pH–distance curve over a 40- $\mu\text{m}$  diameter silver iodide target. The inflection on the pH–distance curve is presumably due to the shielding effect of the tip (15- $\mu\text{m}$  diameter) on the target at small  $d$ . As a control, the pH–distance curves were also recorded in cyanide-free solutions containing potassium chloride in 100 mM concentration. No measurable difference could be observed in this experiment between the pH of the bulk and the target surface. This result provides unequivocal evidence that this corrosion reaction involves a local pH change.

A two-dimensional image of a silver iodide disk (approximately 40- $\mu\text{m}$  diameter) is shown in Figure 12. The image was prepared in unbuffered 1 mM potassium cyanide solution with 0.1 M potassium chloride as background electrolyte. The position of the silver iodide disk is clearly visible in the center of the image. The silver iodide target was slightly elliptical

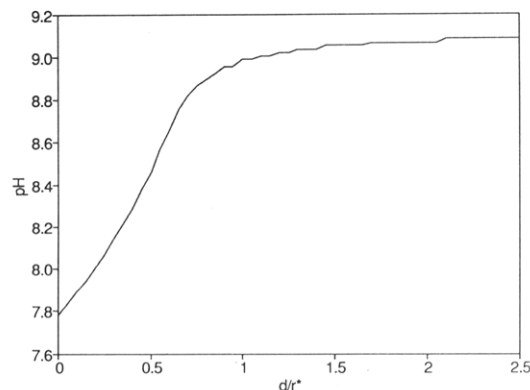


**Figure 11.** pH profile over a 40- $\mu\text{m}$ -diameter silver iodide target. The antimony tip diameter was 15  $\mu\text{m}$ . The solution contained 0.1 M KCl, 1 mM pH 9.0 phosphate buffer, and 1 mM KCN. The x-axis is the tip–surface distance normalized by the radius of the silver iodide target.

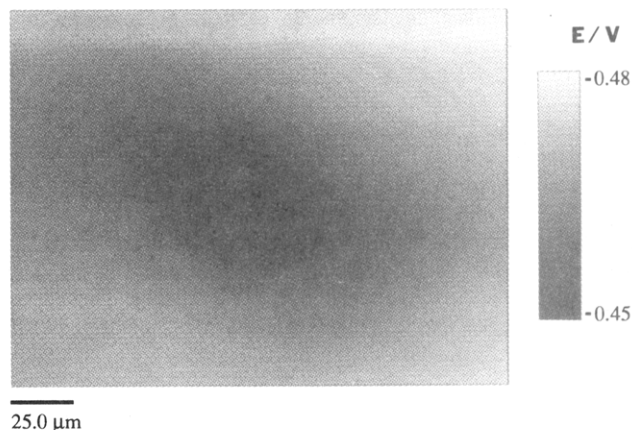


**Figure 12.** Image of the pH profile around a 40- $\mu\text{m}$ -diameter silver iodide target. The gray scale shows the antimony tip potential; white corresponds to higher pH. The tip diameter was 15  $\mu\text{m}$ , the tip scan rate was 10  $\mu\text{m}/\text{s}$ , and the solution contained 0.1 M KCl, 1 mM KCN, and no phosphate buffer.

due to the necessity of heating the glass capillary during filling with silver iodide. The pH over the center of the disk is roughly 8, compared to a value close to 9 in the bulk solution. This demonstrates the applicability of the technique in the study of corrosion processes. More detailed studies of this system will be presented in a separate paper.<sup>31</sup>

**Immobilized Urease.** Local measurement of enzyme activity is important, because there is considerable interest in the use of immobilized enzymes for chemical transformations as well as in analytical chemistry. While amperometric SECM can be used with redox enzymes,<sup>13</sup> the availability of potentiometric SECM widens the range of applications to many other enzymes, e.g., the hydrolases. To investigate the utility of potentiometric SECM in this area, imaging of the local pH change due to the enzyme-catalyzed hydrolysis of urea was attempted. Urease was immobilized in the glass capillaries in a cross-linked gel using bovine serum albumin (BSA) as a matrix and glutaraldehyde as a cross-linking agent. First, the empty capillary was dipped into a 25% aqueous solution of glutaraldehyde, filling the tube with a small amount of glutaraldehyde by capillary action. The tube was wiped on a piece of tissue paper to remove the excess. The cross-linked gel was formed by dipping the end of the tube into a solution of urease and BSA for about 5 min. The enzyme solution contained 20 mg BSA and 5 mg urease in 0.2 mL 0.1 M pH 7.0 phosphate buffer. After this procedure, the tube contained a solid gel of cross-linked protein. To remove the

(28) Mascini, M. *Anal. Chem.* 1973, 45, 614.

(29) Gratzl, M.; Rakias, F.; Horvai, G.; Toth, K.; Pungor, E. *Anal. Chim. Acta* 1978, 102, 85.

(30) Toth, K.; Pungor, E. *Anal. Chim. Acta* 1970, 51, 221.

(31) Nagy, G.; Toth, K.; Horrocks, B. R.; Bard, A. J., manuscript in preparation.

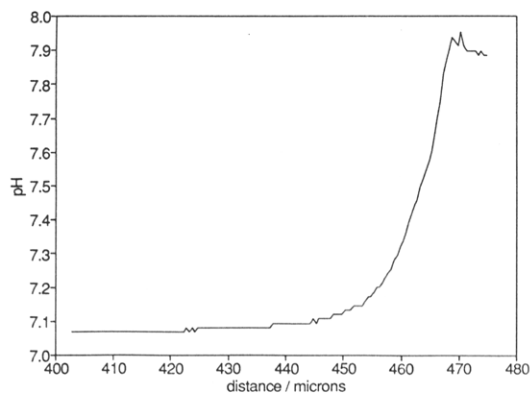
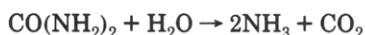


**Figure 13.** pH profile over a 50- $\mu\text{m}$ -diameter immobilized urease target. The antimony tip diameter was 6  $\mu\text{m}$ , and the solution contained 5 mM urea, 0.1 M KCl, and 1 mM pH 7.0 phosphate buffer.

excess glutaraldehyde, the end of the tube was soaked in a 10 mM solution of asparagine in pH 7.0 phosphate buffer. After roughly 30 min, the target was ready for use. After curing, the enzyme gel had shrunk and recessed in the glass tube end by roughly 10–20  $\mu\text{m}$ . Although the target did not have ideal geometry, the enzyme was active.

The urease target was mounted in the cell as for the AgI experiments, and the experimental procedure was as before with a slight modification. The potential of the antimony tip was checked before and after addition of urea to the solution to ensure that no significant hydrolysis of the urea stock solution had occurred. Fresh stock solutions of urea in pH 7.0 buffer were prepared each day. Figure 13 shows a pH-distance profile in the  $z$  direction over the center of a 50- $\mu\text{m}$  diameter urease target in 1 mM pH 7.0 phosphate buffer in the presence of 5 mM urea. No pH profile was observed in the absence of urea or when the tip was far from the enzyme gel disk. It is well-known that urease catalyzes the hydrolysis of urea:



A consideration of the dissociation constants of these species indicates that if the solution is initially at pH 7.0, an increase in pH will occur on hydrolysis. In fact, pH sensors coated with urease have been used as urea sensors.<sup>32,33</sup> The result of Figure 13 shows that local enzyme catalysis can be detected by potentiometric SECM. The hydrogen ion concentration profile calculated from Figure 13 is shown in Figure 14. The inflection point divides the experimental curve into two distinct portions. The first one, between 400 and about 460  $\mu\text{m}$ , represents tip-substrate separations sufficiently large to avoid any tip effect on the substrate reaction. As expected, this portion of the curve fits the theory quantitatively. The portion of the curve after the inflection is disturbed, and the eventual leveling of the proton concentration apparently indicates the tip touching the substrate. The agreement between theory and experiment is better than in Figure 7, because the smaller tip resulted in less stirring or blocking of the diffusion layer over the substrate. An absolute distance scale in this case could not be established because of the uncertainty of the substrate shape, but the flux value found from the curve ( $2.6 \times 10^{-15}$  mol/s) seems reasonable for this size of enzyme-covered surface.

A pH image of a section of a 120- $\mu\text{m}$  diameter urease disk is shown in Figure 15. The whole image could not be captured because the diffusional broadening resulted in a profile that was larger than the maximum scan size currently available

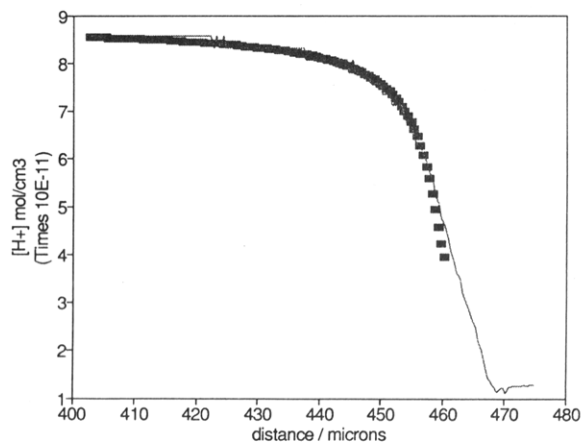


**Figure 14.** Hydrogen ion concentration versus distance derived from the data of Figure 13. The solid line is experimental data, and the filled squares are theoretical data.

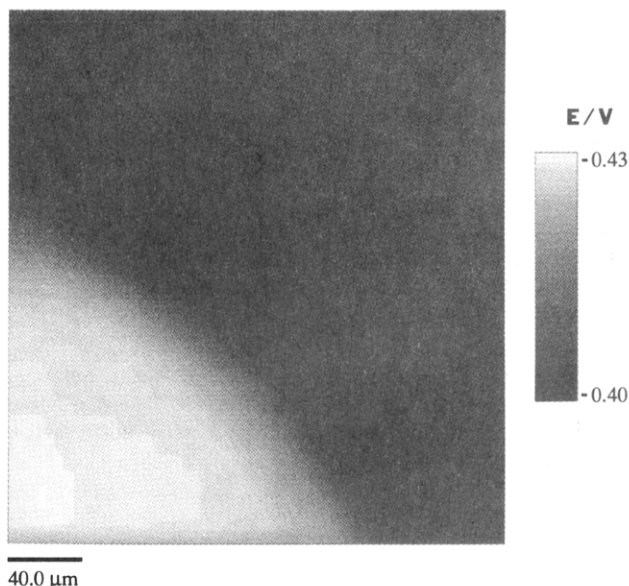


**Figure 15.** Image of the pH profile around a 120- $\mu\text{m}$ -diameter urease gel target. The gray scale shows the antimony tip potential; white corresponds to high pH. The tip diameter was 40  $\mu\text{m}$ , the tip scan rate was 10  $\mu\text{m}/\text{s}$ , and the solution contained 10 mM urea, 0.1 M KCl, and 2 mM pH 7.0 phosphate buffer.

on our instrument. The center of the enzyme target is near the lower left-hand corner of the image where the potential of the antimony tip is 0.43, corresponding to a pH of roughly 7.5. These results show that potentiometric SECM can be used to determine the distribution of enzyme activity on a surface. In principle, different enzymes on the same surface could be separately mapped in solutions of their respective substrates.

**Immobilized Yeast Cells.** An exciting application of SECM with pH sensing tips which can be foreseen is the mapping of pH changes due to the metabolic activity of living systems such as cells, living tissue, or associates of microorganisms. Because of its high metabolic rate, yeast was chosen as the model system to demonstrate the applicability of the technique.

The yeast target was prepared by entrapment of ordinary moist baker's yeast in low gelling temperature agarose.<sup>34</sup> A 3% sample, by weight, of agarose in pH 7.0 buffer was heated in a water bath until a clear solution was obtained. About 1 mL of this solution was allowed to cool slowly to 30–40  $^\circ\text{C}$ .

(32) Guilbault, G. G.; Montalio, J. G. *J. Am. Chem. Soc.* 1969, 91, 2164.

(33) Vadgama, P. In *Ion Selective Electrode Methodology*; Covington, A. K., Ed.; CRC Press: Boca Raton, FL, 1979; Vol. II.

(34) Tampion, J.; Tampion, M. D. *Immobilized Cells*; Cambridge Studies in Biotechnology 5; Cambridge University Press: Cambridge, 1987.

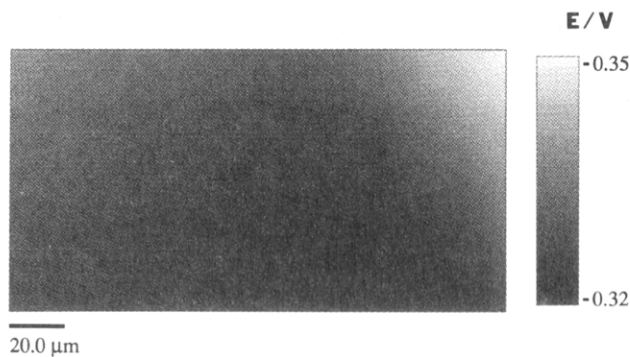


**Figure 16.** Image of the pH profile around a 80- $\mu\text{m}$ -diameter yeast/agarose target. The gray scale shows the antimony tip potential; white corresponds to high pH. The tip diameter was 20  $\mu\text{m}$ , the tip scan rate was 10  $\mu\text{m}/\text{s}$ , and the solution contained 25 mM glucose, 0.1 M KCl, and 1 mM pH 7.0 phosphate buffer.

A small amount of yeast was homogenized in this solution by stirring with a glass rod until a slightly turbid suspension was produced. The turbid suspension was decanted off the sediment. A glass capillary was back-filled with the suspension using a syringe to apply sufficient pressure to force a small droplet out of the end. The target was then allowed to gel at room temperature. To avoid desiccation of the yeast, the target was kept in a sample vial saturated with water vapor. Before use, the droplet of gel protruding from the surface of the target was removed by carefully wiping with a piece of tissue paper to leave only a small disk of gel exposed. The surface of the gel disk was examined, and individual yeast cells could be observed and counted with an optical microscope. The yeast cells were roughly 6  $\mu\text{m}$  long and 3  $\mu\text{m}$  wide.

The target was mounted as before, and the experiment was carried out in pH 7.0 phosphate buffer with the addition of glucose as a metabolic supply. A significant decrease of pH was observed near the target surface. No effect was seen in the absence of yeast cells or glucose. This pH decrease was therefore due to the conversion of glucose to acidic metabolites, most likely carbon dioxide, by the yeast cells. An image of a section of the pH profile across an 80- $\mu\text{m}$  yeast/agarose disk is shown in Figure 16. The center of the yeast disk is toward the lower right-hand corner of the image. Near the center of the target the pH has fallen to ca. 6.3 compared to the value of 7.0 for the bulk of solution. This indicates that the metabolic activity of the immobilized yeast target can be mapped. By examining the target under an optical microscope, it was determined that this pH change was created by approximately 200 individual cells (counting only cells on the surface of the target). Because the pH change observed is fairly large, this technique should be useful in the study of smaller numbers of cells.

## CONCLUSIONS

Antimony-based pH-sensing microelectrodes were employed in SECM to study the possible range of application of potentiometric measurements with this technique. On the basis of these preliminary experiments, we have shown that pH changes occurring during electrochemical reactions, corrosion processes, biocatalytic reactions, and metabolic processes of microorganisms can be successfully mapped on a micrometer scale.

## ACKNOWLEDGMENT

The support of this work by a grant from the National Science Foundation (CHE 9214480) is gratefully acknowledged.

## LIST OF SYMBOLS

$a$	tip radius
$C, c$	concentration of the electroactive species as a function of spatial coordinates and the same variable in dimensionless form
$C^*$	bulk concentration
$D$	diffusion coefficient
$E$	potential of the tip electrode
$J, j, f$	diffusion flux from the substrate surface, its density, and dimensionless flux density, respectively
$J_0$	Bessel function of the first kind of order zero
$K(k)$	complete elliptic integral of the first kind
$K$	dissociation constant
$R, Z$	spatial coordinates; for a hemispherical substrate, $R$ is the polar radius
$r, z$	$R/r^*$ and $Z/r^*$ , respectively
$r^*$	substrate radius
$[X]$	concentration of species X participating in a buffer equilibrium

## APPENDIX

In this appendix the concentration profile above a microdisk electrode generating a constant total flux of material is derived by solving eq 4. The following dimensionless variables will be used

$$r = R/r^*; z = Z/r^*; c = C/C^* - 1; f = -\partial c/\partial z = jr^*/(C^*D) \quad (\text{A1})$$

(normalization of the concentration is possible only if  $C^* \neq 0$ , otherwise  $c = C$ , and the  $C^*$  term should be removed from subsequent expressions). Reproducing the sequence of operations described in ref 35 (but without applying the Laplace transformation because the present problem is time-independent) one obtains:

$$c(r,z) = \int_0^1 uf(u) du \int_0^\infty \exp(-pz) J_0(pr) J_0(pu) dp \quad (\text{A2})$$

where  $J_0$  is the Bessel function of the first kind of order zero.<sup>36</sup>

Equation A2 can be simplified by the substitution<sup>37</sup>

$$\int_0^\infty \exp(-pz) J_0(pr) J_0(pu) dp = \frac{2K(k)}{\pi \sqrt{z^2 + (r+u)^2}} \quad (\text{A3})$$

where  $K(k)$  is the complete elliptic integral of the first kind<sup>36</sup> and  $k = [2\sqrt{ru}]/\sqrt{z^2 + (r+u)^2}$ . Thus

$$c(r,z) = (2/\pi) \int_0^1 \sqrt{u/r} f(u) k K(k) du \quad (\text{A4})$$

Now the function  $f(r)$  needs to be defined. The analogous problem arises in chronopotentiometry with a microdisk electrode<sup>38</sup> when the total flux to the electrode surface is known rather than its radial distribution. There are two approaches to this problem.

(i) The constant flux approximation,<sup>38</sup> i.e., the flux is assumed to be constant across the disk, so that  $f = \text{const} =$

(35) Mirkin, M. V.; Bard, A. J. *J. Electroanal. Chem. Interfacial Electrochem.* 1992, 323, 1.

(36) Abramowitz, M.; Stegun, I. *Handbook of Mathematical Functions*; Dover: New York, 1965.

(37) Gradshteyn, I. S.; Ryzhik, I. M. *Table of Integrals, Series and Products*; Academic: New York, 1965; p 709.

(38) Fleischmann, M.; Pons, B. S. *J. Electroanal. Chem. Interfacial Electrochem.* 1988, 250, 257.

$J/\pi C^* D r^*$ ), leading to

$$c(r,z) = (2f/\pi) \int_0^1 \sqrt{u/r} k K(k) du \quad (\text{A5})$$

The practically important value is  $c(0,z)$  corresponding to a small tip electrode positioned over the center of the substrate. In this case,  $K(0) = \pi/2$ , and

$$c(0,z) = 2f(\sqrt{z^2 + 1} - z) \quad (\text{A6})$$

(39) Nanis, L.; Kesselman, W. *J. Electrochem. Soc.* **1971**, *118*, 454.

(40) Newman, J. In *Electroanalytical Chemistry*; Bard, A. J., Ed.; Marcel Dekker: New York, 1973; Vol. 6, p 187.

in agreement with ref 39 where the same result was obtained in a different way.

(ii) The constant concentration assumption where the flux varies with  $r$  according to the primary current distribution<sup>40</sup>

$$f(r) = 0.5f/\sqrt{1-r^2} \quad (\text{A7})$$

where the average dimensionless flux density,  $f$ , is given above. With this assumption the concentration profile is

$$c(r,z) = (f/\pi) \int_0^1 \sqrt{u/r(1-u^2)} k K(k) du \quad (\text{A8})$$

Received November 25, 1992. Revised manuscript received January 20, 1993. Accepted January 21, 1993.